Increase with energy of parton transverse momenta in the fragmentation region in DIS and related phenomena.

B. Blok[1]†, *L. Frankfurt*[2], *M. Strikman*[3]
[1]Physics department, Technion, Haifa, Israel
[2]Institute School of Physics and Astronomy, Tel Aviv University, Tel Aviv, Israel,
[3]Physics Department, Pensilvania State University, College Station, USA.

Abstract
We demonstrate the fundamental property of pQCD: smaller is the size of the colorless quark-gluon configurations, more rapid is the increase of its interaction with energy. In the limit of fixed Q^2 and $x \to 0$ we find the increase with the energy of the transverse momenta of the quark(antiquark) within the $q\bar{q}$ pair produced in the fragmentation region by the strongly virtual photon. Practical consequences of discovered effects is that the ratio of DVCS to DIS amplitudes should very slowly tend to one at very large collision energies, that a rapid projectile has the biconcave shape, which is different from the expectations of the preQCD parton model where a fast hadron has a pancake shape. We found dominance of different phases of chiral and conformal symmetries in the central and peripheral pp, pA, and AA collisions.

1 Introduction.

A leading order dipole approximation Ref. [1–5], provides the solution of the equations of QCD in the kinematics of fixed and not too small $x = Q^2/\nu$ but $Q^2 \to \infty$. The characteristic feature of this solution is the approximate Bjorken scaling for the structure functions of DIS, i.e. the two dimensional conformal invariance for the moments of the structure functions. In this approximation as well as within the leading $\log(x_0/x)$ approximation, the transverse momenta of quarks within the dipole produced by the local electroweak current are restricted by the virtuality of the external field:

$$\Lambda^2 \leq p_t^2 \leq Q^2/4. \tag{1}$$

Here $\Lambda \equiv \Lambda_{QCD} = 300$ Mev is a QCD scale. It follows from the QCD factorization theorem proved in Refs. [6, 7] that within this kinematical range the smaller transverse size d of the configuration (the transverse distance between the constituents of the dipole) corresponds to a more rapid increase of its interaction with the collision energy:

$$\sigma = \alpha_s(c/d^2)F^2\frac{\pi^2}{4}d^2xG_T(x, c/d^2), \tag{2}$$

here $F^2 = 4/3$ or $9/4$ depends whether the dipole consists of color triplet or color octet constituents, G_T is an integrated gluon distribution function and c is a parameter $c = 4 \div 9$. It is

† speaker

well known in the DGLAP approximation that the structure function $G_T(x,Q^2)$ increases more rapidly with $1/x$ at larger Q^2. This property agrees well with the recent HERA data. The aim of the present talk is to demonstrate that the transverse momenta of the (anti)quark of the $q\bar{q}$ pair produced by a local current increase with the energy and become larger than $Q^2/4$ at sufficiently large energies. In other words the characteristic transverse momenta in the fragmentation region increase with the energy. Technically this effect follows from the more rapid increase with the energy of the pQCD interaction for smaller dipole and the k_t factorization theorem.

It is worth noting that this kinematics is very different from the central rapidity kinematics where the increase of p_t^2 was found in the leading $\alpha_s \log(x_0/x)$ BFKL approximation [8]: $\log^2(p_t^2/p_{t0}^2) \propto \log(s/s_0)$. Indeed, the latter rapid increase is absent in a fixed order of perturbation theory, and is the property of the ladder: the further we go along the ladder, the larger are characteristic transverse momenta, i.e. we have a diffusion in the space of transverse momenta [8]. On the other hand the property we are dealing here with is the property of a characteristic transverse momenta in the wave function of the projectile.

The dipole approximation provides the target rest frame description which is equivalent to the Infinite Momentum Frame (IMF) description of DIS in LO DGLAP and BFKL approximations. To achieve equivalence with the IMF description in the NLO approximation it is necessary to calculate radiative corrections to cross section in the fragmentation region, i.e. to take into account the increase of the number of constituents and related renormalization of the dipole wave function. Recent calculations [9, 10] suggest that these corrections are small. Consequently in the talk we will neglect these corrections.

Our main result is that the median transverse momenta k_t^2 and invariant masses of the leading $q\bar{q}$ pair in the fragmentation region grow as

$$\begin{aligned} k_t^2 &\sim a(Q^2)/(x/x_0)^{\lambda(Q^2)}, \\ M^2 &\sim b(Q^2)/(x/x_0)^{\lambda_{\rm M}(Q^2)}. \end{aligned} \tag{3}$$

Here k_t^2 and M^2 are the median squared transverse momentum and invariant mass of the quark-antiquark pair in the fragmentation region. (The median means that the configurations with the momentum/masses less than the median one contribute half of the total crosssection). The exponential factors λ and $\lambda_{\rm M}$ are both approximately ~ 0.1. These factors are weakly dependent on the external virtuality Q^2. The exact values also depend on the details of the process, i.e. whether we consider the DIS process with longitudinal or transverse photons, as well as on the model and approximation used. The exact form of $\lambda(Q^2)$, and $\lambda_{\rm M}(Q^2)$ are given below.

The rapid increase of the characteristic transverse scales in the fragmentation region has been found first in Refs. [11–14], but within the black disk regime (BDR). Our new result is the prediction of the increase with energy of the jet transverse momenta in the fragmentation region/the rise of the transverse momenta in the impact factor with the energy, in the kinematical domain where methods of pQCD are still applicable. This effect could be considered as a precursor of the black disk regime indicating the possibility of the smooth matching between two regimes.

Our results can be applied to a number of processes. First we consider the deeply virtual Compton scattering (DVCS) process, i.e. $\gamma + p \to \gamma^* + p$.

We also find that at sufficiently large energies

$$\sigma_L(x,Q^2)/\sigma_T(x,Q^2) \propto (Q^2/4p_t^2) \propto (1/x)^\lambda. \tag{4}$$

Hence the σ_L/σ_T ratio should decrease as the power of energy instead of being $O(\alpha_s)$.

Our results have the implication for the space structure of the wave packet describing a rapid hadron. In the classical multiperipheral picture of Gribov a hadron has a shape of a pancake of the longitudinal size $1/\mu$ (where μ is the scale of soft QCD) which does not depend on the incident energy [17]. On the contrary, we find in section 5 the biconcave shape for the rapid hadron in pQCD with the minimal longitudinal length (that corresponds to small impact parameter b) decreasing with increase of energy and being smaller for nuclei than for the nucleons.

Finally, in the last section we discuss the possible applications of our results to pp, pA collisions at the LHC.

2 The target rest frame description.

Within the LO approximation the QCD factorization theorem allows to express the total cross section of the scattering of the longitudinally polarized photon with virtuality $-Q^2 \gg \Lambda^2_{QCD}$ off a hadron target as the convolution of the square of the virtual photon wave function calculated in the dipole approximation and the cross section of the dipole scattering off a hadron [1, 18, 19]. In the target rest frame the cross section for the scattering of longitudinally polarized photon has the form :

$$\sigma(\gamma^*_L + T \to X) = \frac{e^2}{12\pi^2}\int d^2p_t dz \left\langle \psi_{\gamma^*_L}(p_t,z)\right| \sigma(s,p_t^2) \left|\psi_{\gamma^*_L}(p_t,z)\right\rangle. \tag{5}$$

Here σ is the dipole crosssection operator:

$$\sigma = F^2 \cdot \pi^2\alpha_s(4p_t^2)(-\vec{\Delta}_t)\cdot xG(\tilde{x} = (M^2+Q^2)/s, 4p_t^2), \tag{6}$$

here $\vec{\Delta}_t$ is the two dimensional Laplace operator in the space of the transverse momenta, and $M^2 = (p_t^2 + m_q^2)/z(1-z)$ is the invariant mass squared of the dipole. In the coordinate representation σ is just a number function, and not a differential operator as in the momentum representation.

Integrating by parts over p_t it is easy to rewrite Eq. 5 with the LO accuracy in the form where the integrand is explicitly positive:

$$\sigma(\gamma^*_L + T \to X) = \frac{e^2}{12\pi^2}\int \alpha_s(4p_t^2) d^2p_t dz \left\langle \nabla\psi_{\gamma^*_L}(p_t,z)\right| f(s,z,p_t^2) \left|\nabla\psi_{\gamma^*_L}(p_t,z)\right\rangle, \tag{7}$$

here

$$f = (4\pi^2/3)\alpha_s(4p_t^2)xG(\tilde{x},4p_t^2). \tag{8}$$

In the derivation we use the boundary conditions that follow from the fact that the photon wave function decreases rapidly in the $p_t^2 \to \infty$ limit and that the contribution of small p_t is the higher twist effect.

Eq. 7 can be explicitly rewritten in terms of integration in k_t^2 and z as

$$\sigma_L(x,Q^2) = 6\pi \frac{\pi\alpha_{\rm e.m.}\sum e_q^2 F^2 Q^2}{12} \int dk_t^2 \alpha_s(4k_t^2) z^2(1-z)^2 \frac{k_t^2}{(k_t^2+Q^2 z(1-z))^4} \cdot g(\tilde{x}, 4k_t^2). \tag{9}$$

where $\tilde{x}$ is given by $(k_t^2/((z(1-z)+Q^2)/s$. Here we take into account explicitly the (rather weak) z-dependence of the integrand.

The similar derivation can be made for the scattering of transverse photon in configurations of spatially small size. In this case the contribution of small p_t region (Aligned Jet Model contribution) is comparable to the pQCD one. The main interest in this paper is in the region of high energies (HERA and beyond) i.e. sufficiently small $\tilde{x}$, and small Q^2, where pQCD contribution dominates because of the rapid increase of the gluon distribution with the decrease of x. We include a contribution of the aligned jet configurations by imposing a cutoff in transverse momenta (see below for the details).

The pQCD contribution into the total cross section initiated by the transverse photon has the form:

$$\begin{aligned} \sigma_T &= 6\pi \frac{\pi\alpha_{\rm e.m.}\sum e_q^2 F^2}{12} \\ &\times \int_0^1 dz \int dk_t^2 \alpha_s(4k_t^2)(z^2+(1-z)^2) \frac{(k_t^4+Q^4 z^2(1-z)^2)}{(k^2+Q^2 z(1-z))^4} \cdot g(\tilde{x}, 4k_t^2). \end{aligned} \tag{10}$$

In the numerical calculations using Eq. 10 we introduced a cutoff in the space transverse momenta $M^2 z(1-z) \geq u, u \sim 0.35$ GeV^2. The contribution of smaller k_t^2 in the total crosssection was calculated using the AJM model.

3 The characteristic transverse momenta in hard fragmentation processes in LO approximation.

Here we carry out the calculations for realistic energies and realistic structure functions. The numerical results indicate that the effects discussed above are manifest even at the energies of the order $s \sim 10^5 \div 10^7$ GeV^2. We want to draw attention that our main qualitatively new result-the increase of the parton transverse momenta in the current fragmentation region should be valid in NLO, NNLO approximations as well because its derivation uses specific property of DGLAP approximation to pQCD -a larger virtuality leads to a more rapid increase of amplitude with energy. We will also consider the extrapolation of our results to energies of the order $s \sim 10^7$GeV^2. These energies are unattainable at existing facilities. The proposed e-p collider at LHC may reach the invariant energies of order 10^6 GeV^2. However these results are interesting from the theoretical point of view- probing the limits of the pQCD. The relation of our results to the processes at the LHC will be discussed in the last section.

Challenging and unresolved problem is how to use resummation methods at extremely small x [20, 21] to evaluate dependence on energy of parton distribution in the current fragmentation region. At x achieved at HERA account of the energy-momentum conservation restricts

the number of possible gluon emissions by one-two. Such emissions are correctly accounted for within NLO, NNLO DGLAP approximation. One can substantiate this point by evaluation of the number of radiated gluons in the multiRegge kinematics [13]. At extremely small x where number of gluon radiations would be sufficiently large and therefore essential impact parameters would exceed radius of a nucleon the intercept of pQCD Pomeron may become independent on Q^2 as a result of diffusion in the space of transverse momenta. This interesting problem is beyond the scope of this paper.

3.1 The longitudinal photons.

In the case of longitudinal photons we have considered the characteristic median/average transverse momenta scale, that corresponds to the half of the total crosssection σ_L. This scale is determined from Eq. 9 by first integrating over z for given k_t, and then analyzing the corresponding jet distribution. In Figure 1 we present the characteristic graphs for the ratio

$$R(k_t^2) = \frac{\sigma(k_t^2)}{\sigma_L}, \tag{11}$$

where $\sigma(k_t^2)$ corresponds to the result of integration of Eq.9 over transverse momenta $\leq k_t^2$. We see from Fig. 1, that for fixed k_t $R(k_t)$ slowly increases with the increase of the energy. The results based on using CTEQ5 parametrization are qualitatively similar, although the increase of median k_t^2 with the energy is more rapid. The energy dependence of median k_t^2 can be described with a very good accuracy by an approximate formula $(x/0.01)^{0.04+0.025\log(Q^2/Q_0^2)}$. Here $Q_0^2 =$ 10 GeV^2,$x_0 \sim 0.01$. The power increases from ~ 0.04 at $Q^2 \sim 5$ GeV^2, to 0.09 at $Q^2 \sim 100$ GeV^2. For CTEQ5 this power increases to 0.1 at $Q^2 = 100GeV^2$ instead of 0.09. This is consistent with the enhanced rate of the increase of CTEQ5 structure functions as compared to the CTEQ6 ones (see below).

These results allow us to estimate the scales, where one expects the appearance of the new QCD regime, i.e. one has to use the k_t factorization approach. Indeed, the DGLAP approximation is based on the strong ordering in all rungs of the ladder, in particular in the first rung (the impact factor in the $4k_t$ factorization language) we must have $4\Lambda^2_{\rm QCD} \leq 4k_t^2 \leq Q^2$. It is clear, this ordering can not hold, once the median $4k_{tm}^2$ becomes of order Q^2. Then we obtain the condition (using CTEQ6 distribution functions):

$$4a(Q^2)/(x/0.01)^{0.04+0.025\log(Q^2/Q_0^2)} \sim Q^2. \tag{12}$$

Here the function a corresponds to the transverse momenta at $x = 0.01$.

The numerical calculations show that for $Q^2 = 5$ GeV^2 one gets from eq. 12 $x \sim 10^{-4}$, for $Q^2 = 10$ GeV^2 one gets $x \sim 10^{-6}$, which may be reached at LeHC. For larger Q^2 we are however beyond the realistic energies: say for $Q^2 \sim 20$ GeV^2 we need $x \sim 10^{-9}$. The use of CTEQ5 gives qualitatively the same results (for $Q^2 = 30$ GeV^2 we obtain $x \sim 10^{-8}$. Thus we may hope to observe the onset of the new regime for the k_t dependence analyzing small x jet distributions at LeHC/LHC. rations.

3.2 Transverse photons

We performed the numerical analysis for the transverse photons using eqs. 9,10 in the same fashion as for the longitudinal photons. In Figure 2 we depicted the characteristic function $R(k_t^2)$ given by Eq. 11 that gives the characteristic momenta as a function of x for several different values of Q^2. The characteristic energy dependence for median k_t^2 is $(x/0.01)^{0.09+0.014\log(Q^2/Q_0^2)}$ where $x_0 = 0.01, Q_0^2 = 10$ GeV^2. The curves in Fig. 2 clearly show that the characteristic momenta increase with the increase of $1/x$, as the corresponding curves slowly shift to the right.

We see that the average transverse momenta for longitudinal photons is significantly larger than for transverse photons. On the other hand, the invariant masses for transverse photons are always significantly larger than $4k_t^2$. This is due to the large contribution of the AJM type configurations with $z \sim 0, 1$ (z is the fraction of the total momentum of the dipole carried by one of its constituents). Since $M^2 = k_t^2/(z(1-z))$, a more slow increase of M^2 than of k_t^2 is consistent with the slow increase of average z towards 1/2, i.e. the symmetric configurations become dominant, but only at asymptotically large energies.

Once again, we can estimate the boundary of the region where the direct DGLAP approach stops being self-consistent. Assuming $k_t^2 \sim Q^2/4$, we obtain that the boundary for $Q^2 = 3, 5, 10$ GeV^2 is reached at $x \sim 10^{-3}, 10^{-4}, 10^{-6}$. For higher Q^2 this boundary lies at unrealistically high energies. The use of the CTEQ5 parametrization gives qualitatively the same results.

So far we considered only perturbative QCD contribution, and the median transverse momentum was determined relative to the total perturbative crosssection, i.e. the one starting from the cut off $u = 0.35$ GeV^2. It is well known that even at HERA energies the contribution of AJM into the total crosssection is significant. The corresponding AJM contribution to the total crosssection is given in fig. 3a. Note that the median k_t^2 at small virtualities at HERA energies significantly decreases if we calculate it using the crosssection that includes both the pQCD and soft (AJM) contributions. For example, at $Q^2 \sim 10$ GeV^2 the median transverse momentum squared decreases by almost a factor of two down to $k_t^2 \sim 0.65$ GeV^2.

4 Deeply virtual Compton scattering.

As the application of the formulae obtained in this paper we shall consider the DVCS processes $\gamma + p \to \gamma^* + p$. We shall show that the slow increase in the median transverse momenta leads to the slow decrease of the ratio $R = A_{\rm DVCS}/A_{\rm CS}$ with energy to the limiting value equal one.

The DCVS amplitude is described in pQCD by the same formula 10 as the amplitude describing total cross section of DIS at given x, Q^2 but with the substitution in Eq.7 of the wave function of virtual photon by wave function of a real photon, i.e. $Q^2 = 0$.

As a result in pQCD R has the form :

$$R_{\rm pQCD} = \frac{\int_0^1 dz \int dM^2 \alpha_s(M^2 z(1-z))(1/(M^2+Q^2)^2) \cdot g(\tilde{x}, M^2).}{\int_0^1 dz \int dM^2 \alpha_s(M^2 z(1-z))((M^4+Q^4)/(M^2+Q^2)^4)) \cdot g(\tilde{x}, M^2).} \qquad (13)$$

Let us note that strictly speaking, we must use the generalized parton distributions (GPD) in Eq. 13. However the difference between gluon GPD and gluon pdf is not large in this case

because fractions carried by gluons in GPD differ by the factor $\approx$ two at moderate x and tend to one at extremely large energies as the consequence of increase of parton momenta with energy. (In fact most of the non-diagonal effect in this approach is included in the wave functions of the initial and final photons.) As a result we may neglect the difference between GPD and distribution functions in the considered kinematics. The numerical analysis of Eq. 13 shows that indeed the ratio R very slowly decreases with the increase of energy due to a slow increase of a ratio M^2/Q^2 discussed in the previous section, and $R \sim 1.6$ for HERA energies.

The result Eq. 13 is however not complete since we neglected the contribution of the AJ configurations. In this paper we take them into account using the AJM model [37] (and references therein, see also Appendix B of this paper). Indeed as we see from Fig. 3a, the AJ configurations give a substantial contribution to the total crosssection of the DIS of the transverse photons. We refer the reader to appendix B and ref. [24] for the discussion of main properties of the AJM. We see that the AJM contribution to the total crosssection is of order 70% at $Q^2 \sim 1$ GeV^2, $x \sim 0.01$.

Rough estimate gives

$$R_{\rm AJM} \approx 2, \tag{14}$$

since the major difference in the amplitudes describing total cross section of DIS and DCVS is in the difference between the wave functions of the virtual and real photons-the factor $\frac{Q^2+M^2}{Q^2} \approx 2$. But in the essential region of integration $M^2 \approx Q^2$. In the framework of the AJM model the ratio of amplitudes of the DVCS to DIS can be calculated within the leading twist approximation as:

$$R_{\rm AJM} = \frac{Q^2+m_0^2}{Q^2}\log(1+\frac{Q^2}{m_0^2}). \tag{15}$$

Here the parameter $m_0^2 = 0.3 - 0.5$ GeV^2 is the cut off parameter $m_0^2 \leq m_\rho^2$, m_ρ is the ρ meson mass.

Combining the pQCD and AJ model contributions we have

$$R = \frac{R_{\rm pQCD}\sigma_T + R_{\rm AJM}\sigma_{\rm AJM}}{\sigma_T + \sigma_{\rm AJM}}. \tag{16}$$

Here the pQCD contribution into the total crosssection σ_T is given by Eq. 10 and the contribution of AJ to the total crosssection is given by AJM - Eq. 15. The results of numerical calculation as a function of x for several values of Q^2 are depicted in Fig. 3b. The ratio R is close to 2 at HERA energies and increases with Q^2 (from 5 to 100 GeV^2 by $\sim 40\%$). This result is in a good agreement with the analysis of the H1 and ZEUS data in Ref. [15] (see in particular Table 4 in Ref. [15]). Our main prediction is that the ratio R should decreases with the rise of energy. It tends to one at asymptotically large energies in agreement with the result for the BDR [25]. However the onset of this regime is very slow. This prediction can be checked experimentally in the study of DVCS processes at LHeC.

Our conclusion on the important role of AJM contribution in DVCS at HERA energies is in the qualitative agreement with the recent experimental data [16] that shows the important role of soft QCD in the diffractive processes in DIS at HERA.

We want to draw attention that agreement between experimental results and theoretical prediction is rather good. This is due to the fact that the interaction of dipole effectively includes the NLO corrections since parton distributions were obtained by fitting the experimental data. Consequently one may hope that NLO corrections to impact factors are relatively small.

Let us stress that the current calculation is preliminary. More detailed calculation should account for the contribution of c-quark, and study in detail the dependence of R on the AJM parameters).

5 The shape of the fast nucleon and nuclei.

The coherence length l_c corresponds to the life-time of the dipole fluctuation at a given energy in the rest frame of the target. Within the parton model approximation the coherence length is $l_c \sim 1/2m_N x$ [26] i.e. it linearly increases with energy. In pQCD as a result of QCD evolution coherence length increases with energy more slowly [27, 28]:

$$l_c = (1/2m_N x)(s_0/s)^{\lambda}. \tag{17}$$

Such energy dependence of the coherence length shows that the wave function of a fast hadron differs in QCD from that in the Gribov picture [17] .

Let us consider the longitudinal distribution of the partons in a fast hadron. In the parton model the longitudinal spread of the gluonic cloud is $L_z \sim 1/\mu$ for the wee partons (where μ is the soft scale) and it is much larger than for harder partons, with $L_z \sim 1/xP_h$ for partons carrying a finite x fraction of the hadron momentum [17]. The picture is changed qualitatively in the limit of very high energies when interactions reach BD regime for $k_t \gg \mu$. In this case the smallest possible characteristic momenta in the frame where hadron is fast are of the order $k_t(BDR)$ which is a function of both initial energy and transverse coordinate, b of the hadron. Correspondingly, the longitudinal size is $\sim 1/k_t(BDR) \ll 1/\mu$. There is always a tail to the much smaller momenta all the way down to $k_t \sim \mu$ which corresponds to the partons with much larger longitudinal size (a pancake of soft gluons corresponding to the Gribov's picture). However at large energies at the proximity of the unitarity limit the contribution of the gluons with $k_t < k_{\rm tb}$ is strongly suppressed . In the BDR this tail is suppressed by a factor $k_t^2/k_t(BDR)^2$ [12, 30]. In the color glass condensate model the suppression is exponential [31].

Since the gluon parton density decreases with the increase of b the longitudinal size of the hadron is larger for large b, so a hadron has a shape of biconcave lens, see Figs. 4(a),4(b)

In the numerical calculation we took

$$|l_z| = 1/k_t(BDR), \tag{18}$$

neglecting overall factors of the order of one (typically in the Fourier transform one finds $\langle z \rangle \sim \frac{\pi}{\langle p_z \rangle}$). We calculated $k_t(BDR)$ for fixed external virtuality $Q_0^2 \sim 40 GeV^2$. Our results are not sensitive to the value of Q_0^2, as the value of Q^2 only enters in the combination $x' = (Q_0^2 + M^2)/s$, and the k_t^2 we found were comparable or larger than $Q_0^2/4$. Indeed, the direct calculation shows that for small b the change of $1/k_t$ if we go between external virtualities of 60 and 5 GeV^2 is less than 5%. Such weak dependence continues almost to the boundary of the picture Fig. 4a,

where $k_t \sim 1$ GeV. Near the boundary the uncertainty increase to $\sim 25\%$, meaning that for large b (beyond those depicted in Fig. 4a) the nucleon once again becomes a pancake and there is a smooth transition between two pictures (biconcave lens and pancake). We want to emphasize here that the discussed above weak dependence of $k_t(BDR)$ on the resolution scale indicates that the shape of the wave function for small x is almost insensitive to the scale of the probe.

We depict the typical transverse quark structure of the fast nucleon in Fig. 4a. We see that it is drastically different from the naive picture of a fast moving nucleon as a flat narrow disk with small constant thickness. (Similar plot for the gluon distribution is even more narrow). Note also that for the discussed small x range $k_t \geq 1\mathrm{G}eV/c$ for $b \leq 1fm$. Since the spontaneous chiral symmetry breaking corresponds to quark virtuality $\mu^2 \leq 1GeV^2$, probably $\sim 0.7\mathrm{G}eV^2$ [33], corresponding to $k_t \sim \sqrt{\frac{2}{3}\mu^2} \sim 0.7\mathrm{G}eV/c$ the chiral symmetry should be restored for a large range of b in the proton wave function for small x.

Let us consider the DIS on the nuclei for the case of external virtualities of the order of several GeV. In this case the shadowing effects to the large extent cancel the factor $A^{1/3}$ in the gluon density of a nucleus for a central impact parameters, b [32], and the gluon density in the nuclei is comparable to that in a single nucleon for $b \sim 0$. Consequently over the large range of the impact parameters the nucleus longitudinal size is approximately the same as in the nucleon at $b \sim 0$.

However for very small x we find large $k_t(BDR)$ corresponding to $4k_t^2(BDR) \geq 40$ GeV^2. This is a self consistent value as indeed for such Q^2 the leading twist shadowing is small.

Accordingly we calculated the shape of the nucleus for the external virtuality $Q^2 \geq 40$ GeV^2. We should emphasize here that taking a smaller virtuality would not significantly change our result for $k_t(BDR)$ (at the same time LT nuclear shadowing reduces a low momentum tail of the k_t distribution as compared to the nucleon case).

In the discussed limit of the small leading twist shadowing, the corresponding gluon density unintegrated over b is given by a product of a nucleon gluon density and the nuclear profile function:

$$T(b) = \int dz \rho(b,z), \tag{19}$$

where the nuclear three-dimensional density is normalized to A. We use standard Fermi step parametrization [34]

$$\rho(r) = C(A)\frac{A}{1+\exp((r-R_A)/a)}, \;\; R_A = 1.1A^{1/3}\mathrm{fm}, a = 0.56\mathrm{fm}. \tag{20}$$

Here $r = \sqrt{z^2+b^2}$, and A is the atomic number. C(A) is a normalization factor, that can be calculated numerically from the condition $\int d^3r\rho(r) = A$. At the zero impact parameter $T(b) \approx 0.5A^{1/3}$ for large A.

The dependence of the thickness of a fast nucleus as a function of the transverse size is depicted in Fig. 4b for a typical high energy $s = 10^7$ GeV^2, $Q^2 = 40$ GeV^2. We see that the nuclei also has a form of a biconcave lens instead of a flat disk. The dependence on the external virtuality for the nuclei is qualitatively very similar to the case of the nucleon. For small b the dependence is very weak (of order 5%) and increases only close to the boundary of the biconcave

lens region where it is of order 20% (and $k_t \sim 1$ GeV). For larger b we smoothly return to the pancake picture.

Note that this picture is very counterintuitive: the thickness of a nucleus is smaller than of a nucleon in spite of $\sim A^{1/3}$ nucleons at the same impact parameter. The resolution of the paradox in the BD regime is quite simple: the soft fields of individual nucleons destructively interfere cancelling each other. Besides for a given impact parameter b, the longitudinal size of a heavy nucleus $1/k_t^{(A)}(BDR) < 1/k_t^{(p)}(BDR)$ since the gluon distribution function in the nuclei $G_A(x,b) > G_N(x,b)$. So a naive classical picture of a system build of the constituents being larger than each of the constituents is grossly violated. The higher density of partons leads to the restoration of the chiral symmetry in a broad b range and much larger x range than in the nucleon case.

6 Experimental consequences.

The current calculations of the cross sections of the hard processes at the LHC are based on the use of the DGLAP parton distributions and the application of the factorization theorem. Our results imply that in the kinematical region of sufficiently small x it is necessary to use the k_t factorization and the dipole model, instead of the direct use of DGLAP.

A similar analysis must be made for the pp collisions at LHC. It has been understood long ago that the probability of pp collisions at central impact parameter is close to 100% (total Γ is close to 1) even for soft QCD, i.e. at lesser energies than those necessary to achieve BDR for the hard interactions. The compatibility of probability conservation with the rapid increase of hard interactions with energy , predicted by QCD, requires the decrease of importance of soft QCD contribution with energy [36]. As a result the hadronic state emerged in pp, pA, AA collisions at sufficiently large energies consists of two phases. Central collisions would be dominated by the strong interaction with small coupling constant - the phase with unbroken chiral and conformal symmetries. On the contrary, the peripheral collisions are dominated by the more familiar phase with broken chiral and conformal symmetries. At these energies the QCD phase at central collisions - with the unbroken chiral and conformal symmetries -will be different from that for the peripheral collisions. This new phenomenon may appear especially important for the central heavy ion collisions at LHC and at RHIC. Quantitative analysis of this problem will be presented elsewhere.

The hard processes initiated by the real photon can be directly observed in the ultraperipheral collisions [35]. The processes where a real photon scatters on a target, and creates two jets with an invariant mass M^2, can be analyzed in the dipole model by formally putting $Q^2 = 0$, while M^2 is an invariant mass of the jets. In this case with a good accuracy the spectral density discussed above will give the spectrum of jets in the fragmentation region. Our results show that the jet distribution over the transverse momenta will be broad with the maximum moving towards larger transverse momenta with increase of the energy and centrality of the γA collision.

We have seen that our results can also describe DCVS processes. The ratio R of DCVS $\gamma^* \to \gamma^*$ and forward amplitudes at $t = 0$ is of order 2 at HERA energies at small external virtualities, and rapidly growing with Q^2. This ratio slowly decreases with the decrease of x.

Finally, our results can be checked directly, if and when the LHeC facility will be built at

CERN.

More detailed version of this work can be found in Ref. [38]

One of us, B.Blok, thanks S.Brodsky for the useful discussions of the results obtained in the paper. This work was supported in part by the US DOE Contract Number DE- FG02-93ER40771 and BSF.

References

[1] S. J. Brodsky, L. Frankfurt, J. F. Gunion, A. H. Mueller and M. Strikman, Phys. Rev. D50 (1994) 3134. .

[2] H. Abramowicz, L. Frankfurt and M. Strikman, Surveys in High Energy Physics, 11 (1997) 51. .

[3] L. Frankfurt, G.A. Miller, M. Strikman, Ann. Rev. Nucl. Part. Sci., 44 (1994) 501. .

[4] B. Blaettel, G. Baym, L. Frankfurt and M. Strikman, Phys. Rev. Lett., 70 (1993) 896. .

[5] J.C. Collins, L. Frankfurt and M. Strikman, Phys. Rev. D56 (1997) 2982. .

[6] S. Catani, M. Ciafaloni, F. Hauptmann, Nucl. Phys. B366 (1991) 135. .

[7] J. Collins, K. Ellis, Nucl. Phys., B360 (1991) 3. .

[8] E. Kuraev, V. Fadin, L. Lipatov, Sov. Phys.-JEP, 44 (1976) 443; 45 (1977) 199. I. Balitsky and L. Lipatov, Sov. J. Nucl. Phys., 28 (1978) 822. .

[9] V.S. Fadin, hep-ph/9807528. .

[10] F. Carporale, A. Papa, A. Sabio Vera, E. J. of Physics,C53 (2008) 525. .

[11] T. C. Rogers, A. M. Stasto and M. I. Strikman, Unitarity Constraints on Semi-hard Jet Production in Impact Parameter Space,"arXiv:0801.0303 [hep-ph]. .

[12] V. Guzey, L. Frankfurt, M. Strikman, M.McDermott, Eur.J. of Physics, C16 (2000) 641. .

[13] L. Frankfurt, M, Strikman and C. Weiss, Ann.Rev.Nucl.Part.Sci.55 (2005) 403-465. .

[14] T. C. Rogers and M. I. Strikman, Hadronic interactions of ultra-high energy photons with protons and light nuclei in the dipole picture," J. Phys. G **32**, (2006) 2041. .

[15] L. Schoeffel, Phys. Lett.,B658 (2007) 33. .

[16] A. Aktas et al, Eur. Phys. J., C48 (2006) 715; S. Chekhanov et al, arXiv:0812.2003 (hep-ex). .

[17] V. N. Gribov, Space-time description of hadron interactions at high-energies. In *Moscow 1 ITEP school, v.1 'Elementary particles'*, 65,1973. e-Print: hep-ph/0006158. .

[18] L. Frankfurt and M. Strikman, Phys. Rept., 160 (1988) 235. .

[19] L. Frankfurt, A.Radyushkin, M. Strikman, Phys. Rev. D55(1997) 98. .

[20] G. Altarelli, S. Forte, R.D. Ball, Nucl. Phys., B621 (2002) 359; B674 (2003) 459. .

[21] M. Ciafaloni, P. Colferai, G.P. Salam, A. M. Stasto, Phys. Lett., 587 (2004) 87; Phys. Rev. D68 (2003) 114003. .

[22] L. Frankfurt, M. Strikman and C. Weiss, Phys. Rev. D **69**, (2004) 114010. .

[23] L. Frankfurt, A. Freund, V. Guzey and M. Strikman, Phys. Lett., B418 (1998) 345; Erratum-ibid, B429 (1998) 414. .

[24] L. Frankfurt, A. Freund and M. Strikman, Phys. Rev. D58 (1998) 114001; Erratum D59 (1999) 119901. .

[25] V. Guzey, L. Frankfurt, M. Strikman,M. McDermott, Phys.Rev.Lett., 87 (2001) 192301. .

[26] B. L. Ioffe, Phys. Lett., B30 (1969) 123. .

[27] Y. Kovchegov and M. Strikman, Phys. Lett., B516(2001) 314. .

[28] B.Blok and L.Frankfurt Phys.Lett.B630 (2005) 49-57. .

[29] B. Blok, L. Frankfurt, M. Strikman, ArXiv:0811.3737 (hep-ph) .

[30] A.H. Mueller, Nucl.Phys.A702 (2003) 65-72. .

[31] A. Dumitru and J. Jalilian-Marian, Phys. Rev. Lett. **89**,(2002) 022301 [arXiv:hep-ph/0204028]. .

[32] L. Frankfurt, V. Guzey and M. Strikman, Phys. Rev. D **71**, (2005) 054001. .

[33] D. Diakonov and V. Y. Petrov, Nucl. Phys. B **272** (1986) 457 . .

[34] A. Bohr and B.R. Mottelson, Nuclear structure, v.1, W.A. Benjamin, New York, 1969. .

[35] L. Frankfurt and M. Strikman, in Phys. Reports, 455 (2008) 105. .

[36] L. Frankfurt , M. Strikman , M. Zhalov Phys.Lett.B616 (2005), 59-75. .

[37] L. Frankfurt and M. Strikman, Nucl. Phys., B316 (1989) 340. .

[38] B. Blok, L. Frankfurt and Mark Strikman, Increase with energy of parton transverse momenta in the fragmentation region in DIS and related phenomena, eprint arXiv:0904.1450 (hep-ph).

.

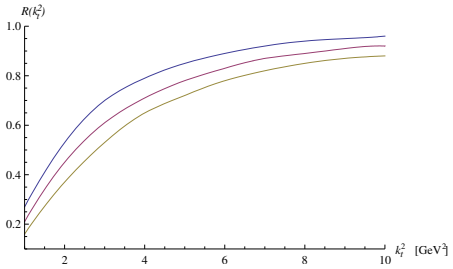

(a) The ratio $R(k_t^2)$ for $Q^2 = 10$ GeV^2 for longitudinal photons. The three curves correspond to x=10^{-3} (upper one), 10^{-5} (middle one) and 10^{-7} (lower one).

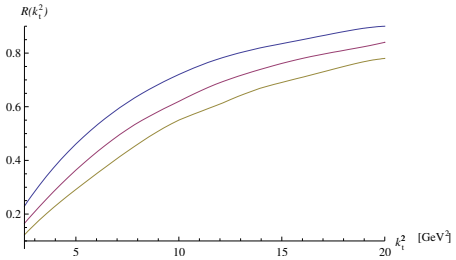

(b) The ratio $R(k_t^2)$ for $Q^2 = 40$ GeV^2 for longitudinal photons. The three curves correspond to x=10^{-3} (upper one), 10^{-5} (middle one) and 10^{-7} (lower one).

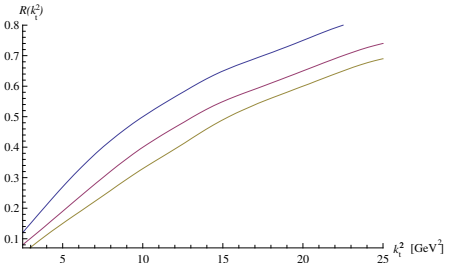

(c) The ratio $R(k_t^2)$ for $Q^2 = 80$ GeV^2 for longitudinal photons. The three curves correspond to x=10^{-3} (upper one), 10^{-5} (middle one) and 10^{-7} (lower one).

Fig. 1: The ratio $R(k_t^2)$ for longitudinal photons for different values of Q^2 and x.

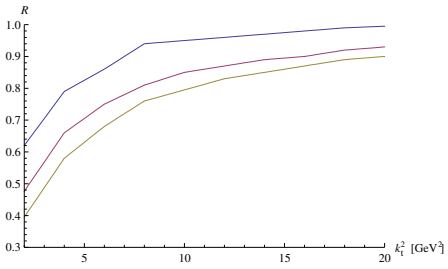

(a) The ratio $R(k_t^2)$ for $Q^2 = 10$ GeV^2 for transverse photons. The three curves correspond to x=10^{-3} (upper one), 10^{-5} (middle one) and 10^{-7} (lower one).

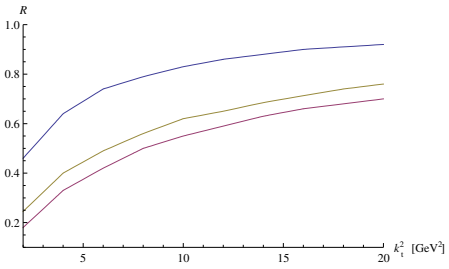

(b) The ratio $R(k_t^2)$ for $Q^2 = 40$ GeV^2 for transverse photons. The three curves correspond to x=10^{-3} (upper one), 10^{-5} (middle one) and 10^{-7} (lower one).

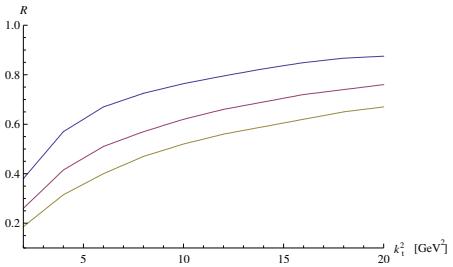

(c) The ratio $R(k_t^2)$ for $Q^2 = 80$ GeV^2 for transverse photons. The three curves correspond to x=10^{-3} (upper one), 10^{-5} (middle one) and 10^{-7} (lower one).

Fig. 2: The ratio $R(k_t^2)$ for transverse photons for different values of Q^2 and x.

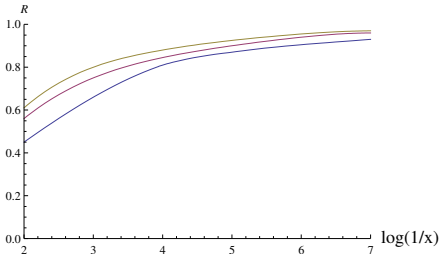

(a) The contribution R of pQCD to the total crosssection, that is a sum of pQCD and AJM model contributions. The cut off of the AJM model is 0.35 GeV^2, for $Q^2 = 5$ GeV^2 (lower curve), 20 GeV^2 (middle curve), 40 GeV^2, the x axis corresponds to $\log_{10}(1/x)$

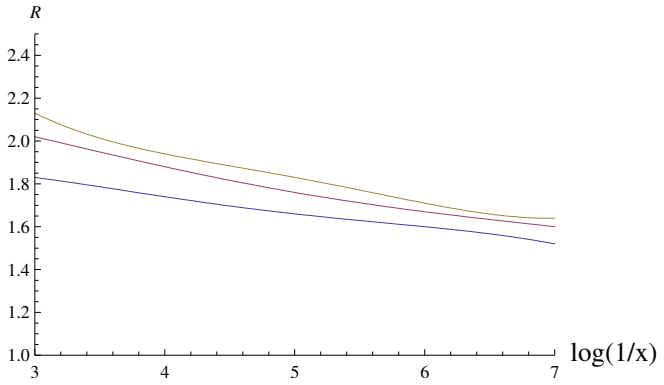

(b) The ratio R of the DVCS crosssection to total transverse crosssection for different values of Q^2 as a function of x_B. for $Q^2 = 5$ GeV^2 (lower curve), 20 GeV^2 (middle curve), 60 GeV^2 (upper curve),the x axis corresponds to $\log_{10}(1/x)$

Fig. 3: The contribution of the AJM to the total crosssection (a), and the the ratio of the DVCS crosssection to a total crossection.

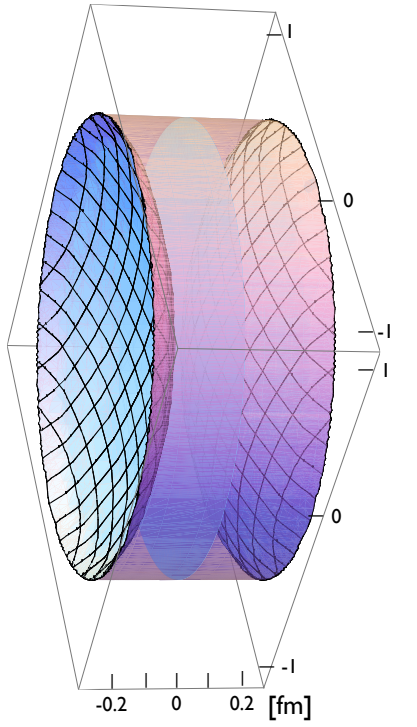

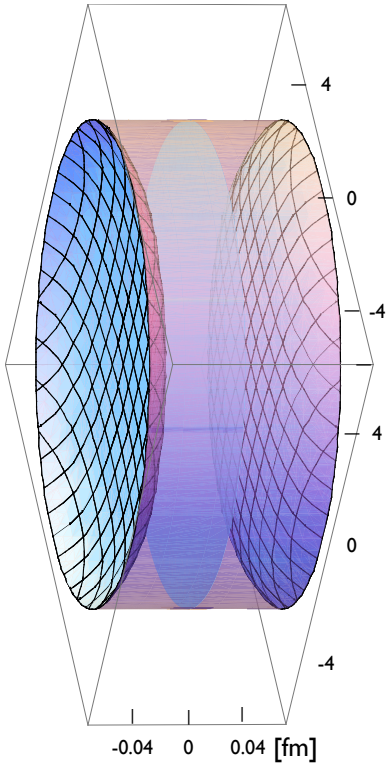

Fig. 4: The shape of the fast nucleon (a) and gold nucleus (b) in QCD at $s = 10^7\,\mathrm{GeV}^2$ and the resolution scale $Q^2 \leq 40\mathrm{GeV}^2$.